Noname manuscript No.
(will be inserted by the editor)

Learning modular and transferable forward models of the motions of push manipulated objects

Marek Kopicki · Sebastian Zurek · Rustam Stolkin · Thomas Moerwald · Jeremy L. Wyatt

Received: date / Accepted: date

Abstract The ability to predict how objects behave during manipulation is an important problem. Models informed by mechanics are powerful, but are hard to tune. An alternative is to learn a model of the object's motion from data, to *learn to predict*. We study this for push manipulation. The paper starts by formulating a quasi-static prediction problem. We then pose the problem of learning to predict in two different frameworks: i) regression and ii) density estimation. Our architecture is modular: many simple object and context specific predictors are learned. We show empirically that such predictors outperform a rigid body dynamics engine tuned on the same data. We then extend the density estimation approach using a product of experts. This allows transfer of learned motion models to objects of novel shape, and to novel actions. With the right representation and learning method these transferred models can match the prediction performance of a rigid body dynamics engine for novel objects or actions.

Keywords Transfer learning · Manipulation · Prediction · Robot Learning

Kopicki is first author. Wyatt, Kopicki and Zurek are the primary authors. Wyatt is corresponding author. We gratefully acknowledge support of grant EU-FP7-IST-600918-PaCMan.

Kopicki, Wyatt et al.
School of Computer Science
University of Birmingham
Birmingham, B15 2TT Tel.: +44-121-414-4788
E-mail: {msk,jlw}@cs.bham.ac.uk

Thomas Moerwald
ACIN, TU Wien
Gusshausstrasse 27-29 / E376 1040 Vienna, Austria
Tel.: +43 (1)58801 - 376631
E-mail: moerwald@acin.tuwien.ac.at

1 Introduction

Prediction is central to intelligent behaviour. An agent must predict its own action effects to be able to plan to achieve its goals (Craik 1943). This paper concerns prediction of the motions of a rigid object when manipulated by a robot. The paper focuses on kinematic models of object behaviour. Within this scope the paper makes the following contributions. First it presents a *modular machine learning* solution to object motion prediction problems, and shows that when tuned for specific objects (or contexts) this approach outperforms physics simulation. Second, it shows transfer of learned motion models to novel objects and actions, with the first results shown for real objects. This ubiquity is precisely what rigid body simulators are designed to achieve. In this paper, we show that, if the right representations are used, transfer learning can even approach the prediction performance of a rigid body simulator on novel objects and actions.

This paper thus extends our previous work (Kopicki 2010; Kopicki et al. 2011) where the core prediction algorithm was presented, and tested mostly in simulation. This paper tests three specific hypotheses, all evaluated with respect to real objects. Hypothesis 1 (H1) is that a *modular learning* approach can outperform physics engines for prediction of rigid body motion. Hypothesis 2 (H2) is that by factorising these modular predictors they can be transferred to make predictions about novel actions. Hypothesis 3 (H3) is that by factorising, learning can be transferred to make predictions about novel shapes. We suppose that learning transfer is only effective given a good representation.

The paper is structured as follows. Section 2 gives a motivation and background. Section 3 describes the problems to be solved, and the modular learning ap-

proach. Next, Section 4 introduces representations of object motion, enabling a formal problem statement in Section 5 and formulation in both regression and density estimation frameworks. Section 6 incorporates contact information, and Section 7 describes how we can factor the learner by the contacts to achieve transfer learning. Section 8 gives implementation details, Section 9 the experimental method, and Section 10 the corresponding results. Section 11 reviews related work. We finish with a discussion in Section 12.

2 The Importance of Prediction for Manipulation

The human motor system uses predictive (or forward) models of the effects that motor actions have on sensory state (Flanagan et al. 2003, 2006; Mehta and Schaal 2002; Witney et al. 2000; Johansson and Cole 1992). The predictions are used for a variety of purposes, including feedforward control, coordination of motor systems, action planning, and monitoring of action plan execution. Neuroscientists have highlighted their importance for dexterous manipulation.

Predictive models also have great utility in robot manipulation. One approach is to build a model informed by theories of mechanics (Mason 1982; Lynch 1992; Lynch and Mason 1996; Peshkin and Sanderson 1988; Cappelleri et al. 2006; Mason 2001; Flickinger et al. 2015), to make predictions of robot and object motion under contact. Various analytic models exist, some making the quasi-static assumption, and others modelling dynamics. To make metrically precise predictions, these models typically require explicit representation of intrinsic parameters of the object and its surroundings, such as friction, mass, mass distribution and coefficients of restitution. These are not trivial to estimate, and even then approximations in the model can render predictions inaccurate. This makes precise, metric predictions out of reach for most cases. Despite the challenges, such a mechanics informed approach has promise, and much useful work on push planning uses either purely kinematic models (Stilman and Kuffner 2008), quasi static models (Dogar and Srinivasa 2010; Lynch and Mason 1996) or rigid body dynamics engines Zito et al. (2012); Cosgun et al. (2011).

A second approach is to learn forward models of object behaviour. Most models have been of qualitative effects (Montesano et al. 2008; Moldovan et al. 2012; Hermans et al. 2011; Fitzpatrick et al. 2003; Ridge et al. 2010; Kroemer and Peters 2014), although metrically precise models have been learned (Meriçli et al. 2014; Scholz and Stilman 2010). These approaches learn action-effect correlations. We extend this to learning the rigid body motions of objects in 3D space, in which objects may twist, slide, topple, and make and break contacts with both the robot and the environment. To achieve this we propose a modular architecture.

3 Three Prediction Problems

To understand hypotheses H1-H3 consider three corresponding prediction problems in Figure 1(a)-(c): action interpolation (P1), action transfer (P2) and shape transfer (P3). Consider how each might be tackled using either: (i) rigid body simulator employing classical mechanics or (ii) statistical machine learning. Assume object and environment shape to be known.

3.1 Action Interpolation (P1).

Supose some pushes of an object were made (Figure 1 (a) top row). In some cases the object tipped, in some it slid. Now a new push direction is tried (bottom row, left column). The task is to predict the new object motion. To do this rigid body mechanics requires parameters such as the object mass and frictional coefficients. These may estimated from the available data. Thus, even for a classical mechanics approach, the problem involves learning. Alternatively, generalisation across actions is feasible using semi- or non-parametric machine learning. This is because the experiences span the test case: there aren't any exactly similar actions, but there are many with similar features. Hence this problem involves *action interpolation*.

3.2 Action Transfer (P2).

Figure 1 (b) depicts a harder problem since the test action (bottom row) now sits outside the range of training actions. Hence this problem is known as *action transfer*. Turning the object around, since it is not symmetric, means that the effects of actions are quite different to before. For example, pushing the top of the L-shaped object will no longer induce it to tip over. This is because the horizontal flap cannot pass through the table: it provides a *kinematic constraint* on the motion of the object. This makes action transfer problems challenging for tabula rasa machine learning. Such problems should, however, be no more challenging for rigid body simulation than problem P1, since once an object's parameters are estimated, the rigid body simulator can produce predictions for any action.

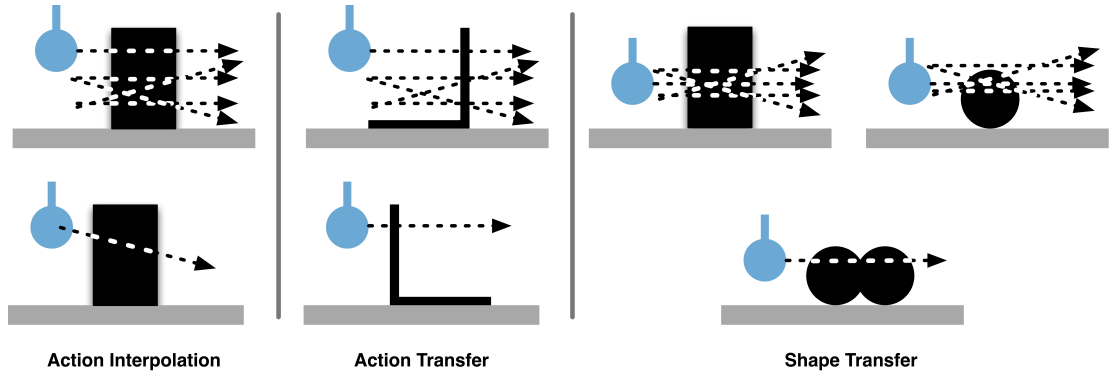

(a) (b) (c)

Fig. 1 Three types of prediction problem. A robot finger is shown in blue, objects in black, and motions of the finger as dashed lines with arrows. Top row: training actions. Bottom row: an example test action. Each column represents a different problem. Sub-figure (a): Problem 1 - Action Interpolation. Subfigure (b): Problem 2 - Transfer to novel actions. Sub-figure (c): Problem 3 - Transfer to novel shapes.

3.3 Shape Transfer (P3).

Finally, Figure 1 (c) requires generalising predictions about action effects to novel shapes. The training data consists of pushes of two objects of different shape. The test action is a push of an object of novel global shape. This is challenging for learning because small changes in object shape can lead to large changes in behaviour. The problem is also challenging for an approach that uses a tuned rigid body simulator, since estimation of mass and frictional coefficients for the test object must be based on the estimates made from the training data, and will thus be sensitive to estimation errors.

Problems P2 and P3 arise from quite different kinds of variation, but in fact are quite similar. Both require a learner to represent the motion types that are possible at contacts. By learning models of contact behaviour, rather than whole object motion, both problems can be solved in essentially the same way.

3.4 The case for modular prediction learning

In this paper we pursue a learning approach to prediction. We could try to learn a single predictor, applicable to wide range of objects and contexts. This is hard, however, because a great deal must be captured in a single learner. Instead we employ a modular prediction scheme, inspired by MOSAIC (Haruno et al. 2001) and other models (Demiris and Johnson 2003). Modular means that the overall prediction engine consists of many context specific predictors (Figure 2), where a context is an object, or an object-environment combination. The first advantage of this is that it can be easier to solve many simple learning problems than one complex learning problem. Second, unobservable parameters (frictional coefficients, mass, mass distribution) need not be modelled explicitly but are instead captured implicitly by being associated with a particular context. Whereas MOSAIC couples control and prediction, it avoids real objects (working with simulated mass spring systems). Our work focuses on pure prediction, but for real objects. Our modular prediction scheme uses vision to distinguish the context, by identifying an object shape from a library.

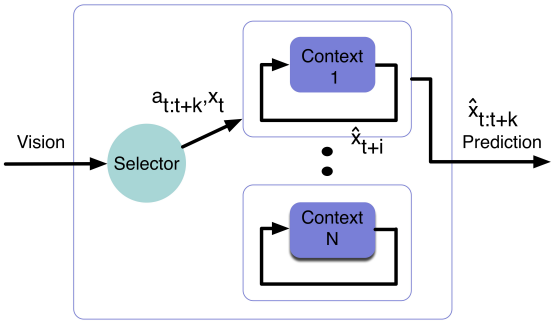

Fig. 2 A modular prediction scheme for solving problem P1. Visual object identification selects a context/predictor, and gives it the object pose and intended finger trajectory as initial input. The chosen predictor takes the current system state x_t and the planned manipulator trajectory $a_{t:t+k}$. The first prediction $\hat{x}_{t+1}$ is fed back on itself to produce a multi-step prediction $\hat{x}_{t:t+k}$.

Having explained our overall scheme, we now turn to the mathematical details of how to model robot-object-environment interactions, which will lead in turn to posing the three prediction problems formally.

4 Encoding rigid body kinematics

We now set up the required notation required. Without loss of generality we explain this using an example

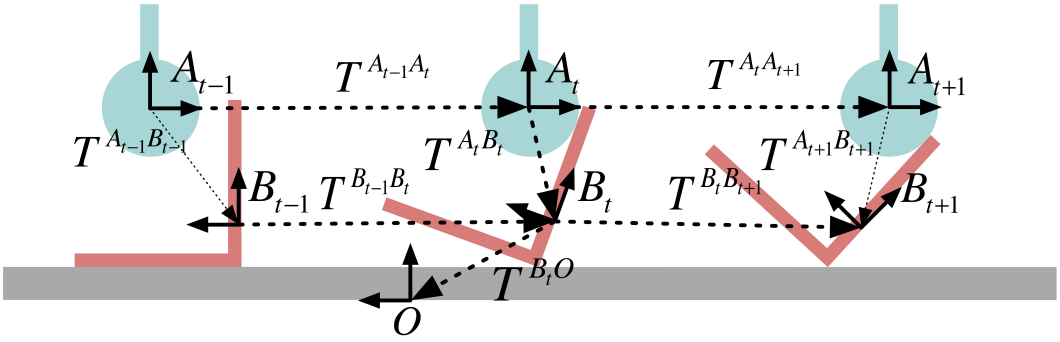

Fig. 3 2D projection at time t of a robotic finger with frame at time t of A_t, an object with frame B_t, and a ground plane with constant frame O. The system can be adequately described using six rigid body transformations. We show all the transformations referred to in the paper, marking the six transformations we use for framing our prediction problem as bold dotted lines, with the others shown as non-bold dotted lines.

from our application domain (Figure 3). Three reference frames A, B and O sit in a 3-dimensional Cartesian space. Frame A is attached to a robot finger which pushes an object with frame B, which in turn is placed on a table top with frame O.[1] While frame O is fixed, A and B change in time and are observed at discrete time steps $..., t-1, t, t+1, ...$ Frame X at time step t is denoted X_t, and the rigid body transformation from a frame X to a frame Y is denoted by $T^{X,Y}$.

From classical mechanics we know that in order to predict the change in state of a rigid body, it is sufficient to know its mass, velocity and a net force applied to the body. We do not assume any knowledge of the mass and applied forces, learning only from object trajectories.[2] We can however, use the motion of a body over time to encode acceleration – an effect of the applied net force. We therefore use rigid body transformations $T^{X,Y}$ of the interacting bodies through time (Figure 3). Given the additional assumption that the net force and the body mass are constant, two subsequent rigid body transformations T^{B_{t-1},B_t} and $T^{B_t,B_{t+1}}$ give a complete description of the state of some body B (here the object) at time step t in the absence of the other bodies. Adding the transformation $T^{B_t,O}$ to give a triple of transformations thus provides a complete description of the state of body B in the fixed frame O (the stationary elements of the environment). Similarly, a second triple of transformations $T^{A_t,O}$, T^{A_{t-1},A_t} and $T^{A_t,A_{t+1}}$ provides such a description for some other body (here the finger) with frame A. The state of the overall system consisting of these two interacting bodies with frames A and B and the fixed environment O can thus be adequately described by these six transformations.

In fact in our representation, we replace transformation $T^{A_t,O}$ by relative transformation T^{A_t,B_t}, thus also explicitly capturing the spatial relationship and thus any contacts between A (finger) and B (object). This gives us a representation consisting of the set of six transformations marked in bold dotted lines in Figure 3. The prediction problem, simply put, will thus be to predict the motion of the object B in the next step: $T^{B_t,B_{t+1}}$ given these five other transformations. Before defining the problem formally, however, we need to think briefly about how best to store these transformations.

Specifically, since we are interested in learning, we need to express this set of transformations in a way that supports generalised predictions. We make extensive use of transformations relative to the frame of the object about which predictions are made. Thus all transformations for learning are expressed in a frame attached to the body of the object, e.g. $T^{X_t,X_{t+1}}_{body}$. At prediction time these transformations are converted into a general inertial frame located in the world, thus becoming for example $T^{X_t,X_{t+1}}_{in}$. This technique is critical to generalisation across inertial frames. In the rest of the paper we will retain subscripts in, but suppress subscripts $body$, and assume that all transformations $T^{X,Y}$ are transformations in the body frame X related to the equivalent transform in some inertial frame using a similarity transform:

$$T^{X,Y} \equiv T^{X,Y}_{body} = (T^{I,X})^{-1} T^{X,Y}_{in} T^{I,X} \quad (1)$$

5 Formal statement: learning to predict

We now have the basics required to formally describe the one-step and then the multi-step prediction problem in such a way that they become problems of learning to predict, and we can effectively tackle Problem 1 (Action Interpolation).

[1] Although it is an abuse of notation, we use A, B and O to denote both the frame and the bodies to which they attach.

[2] We could include forces, and sense them with an F/T sensor. This is future work.

5.1 One step prediction.

The one step prediction problem is formulated as follows: given that we observe the recent and current positions of the finger and object, and know the planned motion of the finger, $T^{A_t,A_{t+1}}$, predict the resulting immediate motion of the object, $T^{B_t,B_{t+1}}$. This is a problem of finding a function f:

$$f : T^{A_t,B_t}, T^{B_t,O}, T^{A_{t-1},A_t}, T^{B_{t-1},B_t}, T^{A_t,A_{t+1}} \longrightarrow T^{B_t,B_{t+1}} \quad (2)$$

The function f is capable of describing the effects of interactions between rigid bodies A and B, provided that their physical properties and net forces are constant in time,[3] in the limit of infinitesimally small time steps. Furthermore, it can be approximately learned from observations for some small fixed time interval Δt between time steps.

If robotic manipulations are performed slowly we can assume quasi-static conditions, and ignore all frames at time $t-1$. This conveniently reduces the dimensionality of the problem, giving a simplified function f_{qs}:

$$f_{qs} : T^{A_t,B_t}, T^{B_t,O}, T^{A_t,A_{t+1}} \longrightarrow T^{B_t,B_{t+1}} \quad (3)$$

5.2 Multi-step prediction.

Having stated the one-step prediction problem it is possible to solve the multi-step prediction problem.[4] Given a predictor (either f or f_{qs}), the initial state of the finger $T^{A_1,O}$ and object $T^{B_1,O}$, and knowing the trajectory of the finger $A_1, \ldots A_T$ over T time steps, one can predict the complete trajectory of the object $B_1, \ldots B_T$, by simply iterating the predictions obtained from f_{qs}. That is, the output of the predictor at time t is used as the input to the predictor for the next time step (Figure 2). While this is a well known approach, it is a hard problem to produce a predictor that will behave well over many time steps. Over time all predictors will diverge from reality. Thus an empirical question is whether for a particular domain and prediction scheme, predictions are reasonably close to reality for a suitable number of steps. It is precisely a multi-step prediction problem that is solved in this paper with the algorithms described below.

[3] A dynamic formulation could explicitly incorporate net forces into the domain and codomain of (2).

[4] In this paper we study the multi-step problem in all our experiments. While the single step problem has been studied for other time series its utility for manipulation planning is low. Second, given fine grained single step predictions it is very hard to distinguish prediction quality over a single step.

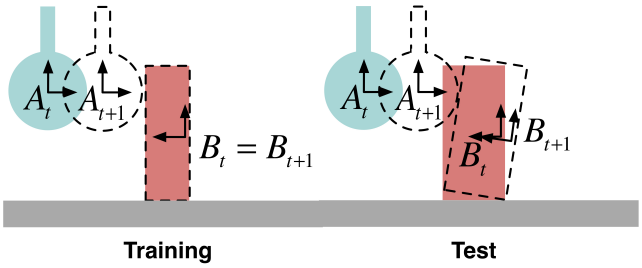

Fig. 4 Two scenes (left and right), each with an object on a tabletop. Only the shape of object B differs between the scenes. Yet when finger A moves as shown by the dashed outline at time $t+1$, the resulting transformation of B will be quite different.

5.3 Learning to predict as regression.

In principle it is straightforward to acquire a predictor f or f_{qs} by learning it from data. Given sufficient experience of object and finger trajectories we can perform a nonparametric regression analysis by taking T^{A_t,B_t}, $T^{B_t,O}, T^{A_t,A_{t+1}}$ as independent variables, and $T^{B_t,B_{t+1}}$ as the dependent variable. Nonetheless a powerful regression technique is needed since the domain of f_{qs} has 18 dimensions or more depending on the parameterisation of motion.

5.4 Learning to predict as density estimation.

As an alternative to learning the mapping (3) by regression, we can recast f_{qs} as a conditional probability density (CPD) p_{qs} over possible object motions $T^{B_t,B_{t+1}}$ (Kopicki et al. 2009):

$$p_{qs}(T^{B_t,B_{t+1}} | T^{A_t,B_t}, T^{B_t,O}, T^{A_t,A_{t+1}}) \quad (4)$$

The learning problem is then posed as one of density estimation, permitting the modelling of the probabilities of many possible outcomes.

Either the regression or density estimation formulation can be used in a modular scheme. In that case a separate module is learned for each combination of agent, object, and environment. Each module interpolates over actions for its context, and thus the system solves problem P1. We now identify the additional information needed to solve problems P2 and P3.

6 Transfer Learning: Representing contacts

The input domains of f, f_{qs}, and p_{qs} are insufficient to pose problems P2 (Action Transfer) or P3 (Shape Transfer). This is because they only capture the *global* relations between objects. To properly pose transfer learning the input domain must capture all the *local*

contact relations between the object and its surroundings. To see why, consider Figure 4. On the left is a training example. On the right is a test case, where the object is wider. Given the same placement of the frames on object and agent, and the same finger motion, the predicted behaviour using Equation (3) will be the same as for the training example. This is wrong. For the correct prediction to be transferred, additional information is needed on the contact between A and B. This can be captured by attaching additional frames to A and B close to their point of contact (see Figure 5, centre panel). In general, an object has multiple contacts with the robot and the environment. Each of these contacts provides a kinematic constraint on the object's motion, and thus each one should be modelled. Rigid body simulators use just such contact information.

We use a pair of local frames to encode each contact or near contact. Each pair encodes one transformation between part of the object B and another body. To distinguish these local frame pairs from what has gone before we henceforth refer to the main frame attached to a body (defined in Section 4) as that body's global frame. We define the local frame pairs as follows. Consider Figure 5 (left panel). We first define a pair of local frames capturing the finger-object contact as A_t^L and B_t^L (centre panel). These are spatially dynamic, i.e. at any time t they are located at the points of closest proximity on the finger and object respectively. We define the *agent-object contact* information as the transformations $T^{A_t^L,A_{t+1}^L}$ and $T^{A_t^L,B_t^L}$.

We also define local frame pairs to model object-environment contacts. One frame is attached to some point on the object (B_t^{Sk}), and one is attached to the nearest point in the environment E_t^{Sk}. Thus the environment frame within each pair is spatially dynamic, changing its position as the object moves. If N points on the object are chosen for modelling there will be N pairs of local frames B_t^{Sk} and E_t^{Sk} to capture the object-environment contacts at time t, where $(k = 1 \dots N)$ (Figure 5 right panel). Using these frame pairs we then define the *object-environment contact* information as the set of transformations $T^{E_t^{Sk},B_t^{Sk}}$ for $k = 1 \dots N$.

During training a single type of contact model is learned by pooling data from frames located at several points on the object. During transfer this single model is copied, creating several identical contact experts on the new object. An extension would be to condition a number of such contact models by the local shapes at the contacts, and this is an intended line of future work. We hypothesize that both data pooling and conditioning will be important elements in improving the transfer of predictions. Additionally, to obtain the results presented in this paper, the number and the locations of the frames B_t^{Sk} on each different object were determined empirically.[5] Finally, we note that we have motivated these contact experts as enabling shape transfer, but they are equally applicable to action transfer. The top row of Figure 6 shows a training and a test case for problem P2 (action transfer). The prediction for the test case requires encoding of the kinematic constraint imposed by the contact between the base of the L-shaped flap and the table. This constraint exists in the training push, but was not significant since the flap could rotate on its corner.

We can now consider the effects that different sets of information might have. A predictor possessed only of global frames for each body we refer to as having global information (G). We add agent-object contact information (G+A), and object-environment contact information (G+A+E). Now consider the possible predictions for the test case (Figure 6 bottom row). A predictor using G will predict that the object will not move. A predictor using G+A has information from the training case that the object surface will move with the finger, so that the finger will not pass through it, but is also capable of predicting that the object rotates about the corner and into the table since it doesn't model the object-environment contact. A predictor using G+A+E will have information about the effect of the contact between the base of the flap and the table and so should avoid predicting a rotation into the table. One point is critical here: the above analysis only concerns what the information allows, it depends on the ability of the learner to utilise it. To test this we must incorporate the information into each learning framework. We can simply extend the regression and density estimation frameworks to achieve this. For regression one way to incorporate the extra information A_t^L,B_t^L and E_t^{Sk},B_t^{Sk}, provided by the agent and environment contacts, is simply to enlarge the domain of function f in Equation (3), that is:

$$f'_{qs} : T^{A_t,B_t}, T^{B_t,O}, T^{A_t,A_{t+1}}, T^{A_t^L,B_t^L} \{, T^{E_t^{Sk},B_t^{Sk}}\}_{k=1\dots N} \longrightarrow T^{B_t,B_{t+1}} \quad (5)$$

Unfortunately, because the dimensionality of the domain of f'_{qs} grows with the number of environment contacts N, the difficulty of learning the mapping f'_{qs} rapidly increases as environment contacts are added.

The conditional probability density (CPD) p_{qs} over possible object motions $T^{B_t,B_{t+1}}$ (Kopicki et al. 2009) is augmented as follows:

$$p_{qs}(T^{B_t,B_{t+1}} | T^{A_t,B_t}, T^{B_t,O}, T^{A_t,A_{t+1}}, T^{A_t^L,B_t^L} \{, T^{E_t^{Sk},B_t^{Sk}}\}_{k=1\dots N}) \quad (6)$$

[5] This procedure could be automated.

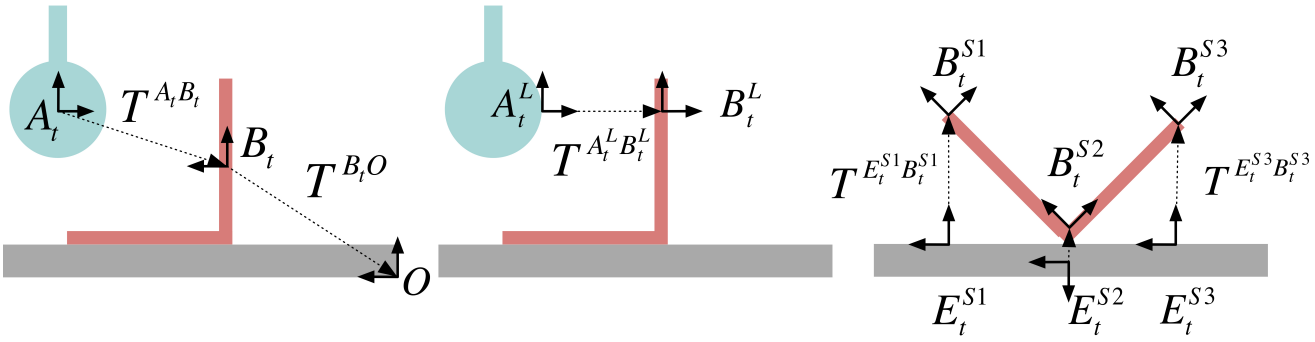

Fig. 5 Three types of information useful in prediction problems. Left: (G - global) global frames of reference for the robot, object and the world. Centre: (A - agent) local frames of reference on the robot finger and the closest point on the object. Right (E - environment) local frames of reference on the object and the closest points on surfaces in the environment.

Again the dimensionality of the conditioning variables makes density estimation hard as the number of contacts grows. One way around this in the density estimation case is to factorize the density in a way that reflects the contact structure. We consider this in the next section.

7 Factorised density estimation

Both formulations give learning problems that increase in difficulty as further contacts are added. One question is whether either formulation can be recast so as to take advantage of the natural problem structure. This section presents one such scheme for the density estimation (or CPD) formulation, based on a product of experts.

Specifically the CPD formulation allows us to factorise the density and approximate p_{qs} by making a conditional independence assumption. The unfactored CPD formulation gives a density over possible one step motions of the object. We can factorise this by breaking up the conditioning variables into groups according to the contacts. This reflects the notion that the behaviour at one contact is independent of the other contacts: each component of the product is an expert encoding the likely object motions given a single kinematic constraint. The product will be maximised by a motion that best satisfies all the constraints simultaneously.

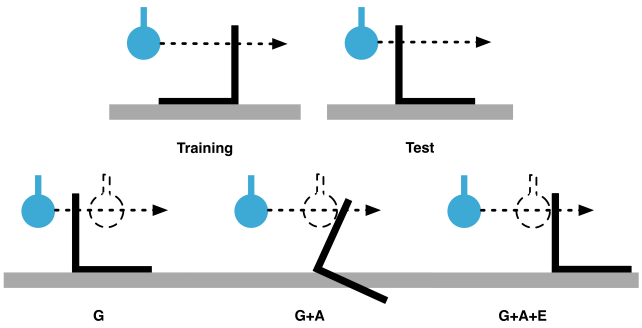

Fig. 6 Information for Action Transfer: an L-shaped object is pushed by a finger. Various predictors are trained solely on forward pushes (top left), but tested on backwards pushes (top right). The top panels show a training and a test push, whereas the bottom panels show predictions given different information (G, G+A and G+A+E) for the test push.

The computational advantage is that since the component densities factorise the conditioning variables of p_{qs} their domains' dimensionalities are smaller, and so potentially they can better manage the complexity of incorporating more information into the predictor. Furthermore, the subset of experts used in the product can be selected dynamically, depending for example on the current set of contacts. Schematically, for some normalisation constant C we propose the following factorisation:

$$p_{qs} \approx C\ p_{global}\ p_{agent} \prod_{k=1\ldots N} p_{env,k} \tag{7}$$

where

$$p_{global} \equiv p_{global}(T^{B_t,B_{t+1}} | T^{A_t,A_{t+1}}, T^{A_t,B_t}, T^{B_t,O}) \tag{8a}$$

$$p_{agent} \equiv p_{agent}(T^{B_t^L,B_{t+1}^L} | T^{A_t^L,A_{t+1}^L}, T^{A_t^L,B_t^L}) \tag{8b}$$

$$p_{env,k} \equiv p_{env,k}(T^{B_t^{Sk},B_{t+1}^{Sk}} | T^{E_t^{Sk},B_t^{Sk}}) \tag{8c}$$

denote the *global*, *agent-object* and k^{th} *object environment* density factors respectively (Kopicki et al. 2009; Kopicki 2010). The one step prediction problem can then be defined as finding the transformation $\widetilde{T}_{in}^{B_t,B_{t+1}}$ expressed in some inertial frame which maximises the product of densities (7):

$$\widetilde{T}_{in}^{B_t,B_{t+1}} = \underset{T_{in}^{B_t,B_{t+1}}}{\operatorname{argmax}} \left\{ p_{global}\ p_{agent} \prod_{k=1\ldots N} p_{env,k} \right\} \tag{9}$$

where similarity transforms as described in Section 4 must be used to evaluate p_{global}, p_{agent} and the N environment factors $p_{env,k}$ for a given $T_{in}^{B_t,B_{t+1}}$.

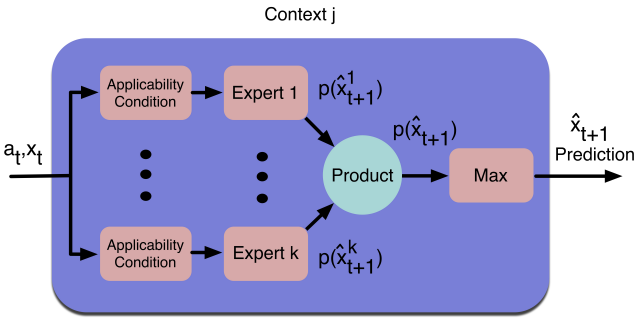

Fig. 7 A Dynamic Product of Experts. This gives the structure of a factorised predictor for a single context as depicted in the modular learner in Figure 2. Each expert in the product has an applicability condition which determines whether it contributes to the product. The applicable predictors combine densities over predictions to produce an overall density. This is optimised to produce a specific prediction.

The key property here is that the global, agent and environment densities encode different information as to which rigid body transformations are feasible. By taking the product of these densities, only transformations which are feasible in all factors' frames will have high probability in the resulting combined distribution. In addition we make this product dynamic in the number of object-environment factors. Once the object surface is beyond some threshold distance from the environment surface its predictor switches off, and when it is close enough it switches on again. This enables us to keep only relevant predictors in the product at any one time – improving prediction quality and efficiency.

In summary we have now described two main formulations (regression and density estimation) able to incorporate varying amounts of information (G, G+A, G+A+E). We have also presented a reformulation of density estimation that factorises the prediction problem given information G+A or G+A+E into a product of experts. Which information and problem formulation should be combined to provide the best prediction framework? Is the factorised problem better able to exploit the additional information than the unfactorised version? These questions can only be answered using specific regression and density estimation algorithms. Having completed our problem formulation we therefore now turn to the details of the implementations we used for each framework.

8 Implementation

The implementations are indexed by the algorithms used, and the information employed. For the function approximation formulation we used Locally Weighted Projection Regression (LWPR). For the unfactored density estimation formulation we used a variant of Kernel Density Estimation (KDE), and for the factored density estimation formulation we also used KDE, but denote it KDEF where -F denotes the use of factorisation. In addition, each algorithm: LWPR, KDE, KDEF, was implemented with differing amounts of input information. We denote these G (Global), GA (Global and Agent) and GAE (Global and Agent and Environment), as described previously. All the implementations depend on the parameterisation of rigid-body transformations chosen. In this paper we tested two parameterisations of orientation: Euler angles and quaternions (see e.g. (Murray et al. 1994)). We also employed two different densities for the quaternion parameterisation: Gaussian and von-Mises Fisher.

8.1 Regression method

LWPR (Vijayakumar et al. 2005) is a powerful method applied widely in robotics, to estimate the mapping described by Equation (3). The regression scheme was implemented using the LWPR software library (Klanke et al. 2008). LWPR was chosen because it employs an incremental learning algorithm that can handle a large number of input dimensions. After initial experimentation LWPR was run using the Euler angle parameterisation. The dimensions of the input and output spaces of each LWPR predictor are summarised in Table 1.

8.2 Kernel density method

A variant of Kernel Density Estimation (KDE) (Scott and Sain 2004) is used to approximate the conditional densities employed in the product in Equation (9). This requires that we encode the rigid body transformations as parameter vectors. To that end, and for the sake of compactness, we introduce some additional notation. First $T^{\mathbf{x}_f}$ is used to denote the set of conditioning transformations for factor $f \in \{G, A, (E,1) \ldots (E,N)\}$, and $T^{\mathbf{y}_f}$ for the corresponding conditioned transformation. $\mathbf{x}_f$ and $\mathbf{y}_f$ are then simply the corresponding parameter vectors for a given parameterisation. Given this the global factor, for example, can be referred to in three equivalent ways:

$$p_G(T^{B_t,B_{t+1}}|T^{A_t,A_{t+1}}, T^{A_t,B_t}, T^{B_t,O}) \quad (10)$$
$$\equiv p_G(T^{\mathbf{y}_G}|T^{\mathbf{x}_G}) \quad (11)$$
$$\equiv p_G(\mathbf{y}_G|\mathbf{x}_G) \quad (12)$$

Finally we define the parameter vectors for the unfactored density estimation problem Eq.(6) as the concatenation of the vectors for each factor, so that

$$\mathbf{x} = \langle \mathbf{x}_G, \mathbf{x}_A, \{\mathbf{x}_{E,k}\}_{k=1...N} \rangle \quad (13)$$

$$\mathbf{y} = \langle \mathbf{y}_G, \mathbf{y}_A, \{\mathbf{y}_{E,k}\}_{k=1...N} \rangle \quad (14)$$

So as to capture the conditional probability densities (CPD) over $\mathbf{y}_f$ for all the different values of $\mathbf{x}_f$ we simply perform kernel density estimation for their joint density, and then index by the specific $\mathbf{x}^t$ at prediction time to give $p_f(\mathbf{y}_f^t|\mathbf{x}_f^t)$. For factor f the joint density kernel estimate is:

$$p_f(\mathbf{y}_f, \mathbf{x}_f) \propto \sum_{j=1...M} K_{\mathbf{H}^{\mathbf{x}_f}}(\mathbf{x}_f - \hat{\mathbf{x}}_f^j) K_{\mathbf{H}^{\mathbf{y}_f}}(\mathbf{y}_f - \hat{\mathbf{y}}_f^j) \quad (15)$$

where the bandwidth matrices $\mathbf{H}^{\mathbf{x}_f}$ and $\mathbf{H}^{\mathbf{y}_f}$ are diagonal, so that $\mathbf{H}_{ii}^{\mathbf{x}_f} = \theta \mathbf{h}_i^{\mathbf{x}_f}$. Vectors $\mathbf{h}^{\mathbf{x}_f}$ and $\mathbf{h}^{\mathbf{y}_f}$ are estimated from training samples using Silverman's "multivariate rule-of-thumb" (Scott and Sain 2004). The additional scaling parameter $\theta \in \mathbb{R}$ is estimated by model selection (see Subsection 9.2). Note that $\mathbf{H}^{\mathbf{x}_f}$ and $\mathbf{H}^{\mathbf{y}_f}$ depend on the factor f being estimated. Given that they are diagonal, and suppressing f and θ for compactness, each kernel function $K()$ in Equation (15) can thus be written:

$$K_{\mathbf{H}^{\mathbf{x}}}(\mathbf{x} - \hat{\mathbf{x}}) = \exp\left[-\frac{1}{2} d(\mathbf{x}, \hat{\mathbf{x}}, \mathbf{h}^{\mathbf{x}})\right] \quad (16)$$

where $d()$ is a *distance function* that determines the kernel type. We employed Gaussian kernels for both Euler and quaternion representations, and additionally Gaussian+Von Mises Fisher kernels for the case of quaternions. For a *Gaussian kernel*:

$$d_{\mathcal{N}}(\mathbf{x}, \hat{\mathbf{x}}, \mathbf{h}) = (\mathbf{x} - \hat{\mathbf{x}})^{\mathrm{T}} \mathbf{H}^{-1} (\mathbf{x} - \hat{\mathbf{x}}) \quad (17)$$

For a product of a Gaussian kernel and *von Mises–Fisher* kernel:

$$d_{\mathcal{N}\mathrm{V}}(\mathbf{x}, \hat{\mathbf{x}}, \mathbf{h}) = d_{\mathcal{N}}(\mathbf{p}, \hat{\mathbf{p}} \mathbf{h}^{(p)}) + d_{\mathrm{V}}(\mathbf{q}, \hat{\mathbf{q}}, h^{(q)}) \quad (18)$$

where $\mathbf{h} = \left[\mathbf{h}^{(p)}; h^{(q)}\right]$, $\mathbf{h}^{(p)} \in \mathbb{R}^3$, $h^{(q)} \in \mathbb{R}$, and (see e.g. (Abramowitz and Stegun 1965)):

$$d_{\mathrm{V}}(\mathbf{q}, \hat{\mathbf{q}}, h^{(q)}) = 2h^{(q)} \left(1 - |\mathbf{q} \cdot \hat{\mathbf{q}}|\right) \quad (19)$$

where $\mathbf{q} \cdot \hat{\mathbf{q}}$ is the quaternion dot product and taking the absolute value fixes the double cover problem. This Von Mises–Fisher kernel is an approximation (up to a multiplicative constant (Detry 2010)) of the von Mises–Fisher distribution.

The learning algorithm for a single context for factored KDE is now straightforward given a set of S training sequences $\{(\hat{\mathbf{x}}^{1:\tau}, \hat{\mathbf{y}}^{1:\tau})_s\}_{s=1...S}$, each of length τ. The kernel centres are simply stored in a set $\mathcal{K} = \{(\hat{\mathbf{x}}_f^j, \hat{\mathbf{y}}_f^j) \forall f \in F\}_{j=1...M}$, where $\hat{\mathbf{x}}_f^j$ denotes the j^{th} kernel centre, and $M = \tau \times S$. A kernel bandwidth is computed for $\mathbf{x}_f$ and $\mathbf{y}_f$ for each factor f, and stored in a set $\mathcal{H} = \{(\mathbf{H}^{\mathbf{x}_f}, \mathbf{H}^{\mathbf{y}_f})\}_{f \in F}$. The training procedure for KDE is identical, but with only one factor. The dimensionality of the input ($\mathbf{x}$) and output ($\mathbf{y}$) spaces for different KDEF predictors is summarised in Table 1. The equivalent unfactored KDE space is obtained by summing over the factors of the equivalent KDEF predictor. Each object is trained as a separate context to form a modular predictor.

Predictor	input dim.			output dim.
LWPR-G (e)	18			6
LWPR-GA (e)	24			6
LWPR-GAE (e)	24 + N*6			6
	global	agent	env	
KDEF (e)	18	12	6	6
KDEF (q)	21	14	7	7
KDEF (v)	21	14	7	7

Table 1 Input & output dimensionality. There are N "environment contacts". There are N environment experts.

8.3 Prediction

Single step prediction for LWPR is straightforward, but single step prediction for KDE involves optimisation of the likelihood of the prediction, and for KDEF this is non-trivial. We describe that here. Following Equation (9), the single step prediction problem can be defined as finding the transformation $T^{\mathbf{y}^*}$, parameterised by $\mathbf{y}^*$, which maximises the product of conditional densities (7) given query $\mathbf{x}$, i.e.:

$$\mathbf{y}^* = \underset{\mathbf{y}}{\operatorname{argmax}}\, p_{qs}(\mathbf{y}|\mathbf{x}) \quad (20)$$

The one-step prediction algorithm is given in Fig 8. First for the input vector $\mathbf{x}$, the conditional density over $\mathbf{y}$ must be obtained for each factor f. This is achieved by evaluation of each kernel $K_{\mathbf{H}^{\mathbf{x}_f}}(\mathbf{x}_f - \hat{\mathbf{x}}_f^j)$ from $j = 1 : M$ in Eq (15) to give a weight $w_{f,j}$. The vector of normalised weights $\mathbf{w_f}$ forms a distribution over the kernels in $\mathbf{y}_f$. $\mathbf{w_f}$ is computed for every factor f. For efficiency we only consider the r kernels with the highest weights $w_{f,j}$ at the query point $\mathbf{x}_f$.

A initial population of solutions is then generated by sampling. First a factor f is sampled randomly. Then a kernel j is sampled by drawing j according to the distribution $\mathbf{w}_f$. Finally a candidate $\tilde{\mathbf{y}}$ is sampled from the j^{th} kernel with centre $\hat{\mathbf{y}}_f^j$. This sampling procedure is run β times to create the initial set of candidate solutions.

one-step-prediction-KDEF(x) $\rightarrow \mathbf{y}^*$
$F = (G, A, (E, 1) \dots (E, N))$
for $f \in F$ **do**
  for $j = 1$ to M **do**
    $w_{f,j} = K_{\mathbf{H^{xf}}}(\mathbf{x}_f - \hat{\mathbf{x}}_f^j)$
  end for
  $\mathbf{w_f}$ = normalisation$(w_{f,1} \dots w_{f,M})$
end for
for $i = 1$ to β **do**
  randomly sample a factor $f \in F$
  sample j from distribution $\mathbf{w_f}$
  $\mathcal{Y}_i = \tilde{\mathbf{y}}$ sampled from density with mean $\hat{\mathbf{y}}_f^j$ and bandwidth $\mathbf{H^{yf}}$
end for
maximise Eq.10 with Y^* = differential-evolution($\mathcal{Y}$,$\mathcal{K}$)

Fig. 8 One-step prediction for the KDEF method

This initial solution set is then refined by stochastic optimisation with respect to p_{qs}. To achieve this similarity transforms must be used to evaluate the likelihood of each $\mathbf{y}$ according to each factor f. Any optimisation routine could be applied, but we used differential evolution (DE) (Storn and Price 1997)[6]. DE is particularly simple to tune, since it is has two meta-parameters: *crossover probability* α and *population size* β. If the number of generations is fixed, the total run time scales linearly with the number of factors, their dimensionality and the number of samples. Optionally, the entire maximisation procedure is stopped when no further significant improvement is observed.

In order to solve the multi-step prediction problem, the prediction from the one step prediction algorithm $\mathbf{y}^t$ is fed back as the relevant part of the conditioning parameter vector $\mathbf{x}^{t+1}$. In this way long prediction sequences can be generated for all the algorithms. For efficiency, no learning or prediction was performed in a given trial until the initial contact was made between the robot and object.

9 Experimental study

9.1 Overview of experiments

We conducted three experiments, one for each problem in Section 3: P1 (action interpolation), P2 (action transfer) and P3 (shape transfer). Each experiment tests all combinations of information (G,A,E) and learning algorithm (LWPR, KDE, KDEF) (see Table 3). The structure of these experiments reflects the structure of our hypotheses: H1-H3.

[6] Note that one cannot use the mean-shift algorithm (Cheng 1995) due to the product involved in (20)

9.1.1 Experiment P1 (action interpolation)

This tests hypothesis **H1***: a modular learning approach can outperform physics engines for prediction of rigid body motion.* Each learning method was used to learn a context/object specific predictor and the results were compared to the predictions of a physics simulator that had also been tuned to each object in a modular manner. We also compared the effects of different parameterisations of rigid body transformations. In addition to the real experiments, we conducted simulation experiments for a cylinder on a non-planar surface.

9.1.2 Experiment P2 (action transfer)

This tests hypothesis **H2***: learned predictions can be transferred to novel actions.* The learners were trained with a reduced action set on a non-symmetric object and then tested on that object with novel actions. We performed this in simulation and with a real object.

9.1.3 Experiment P3 (shape transfer)

This tests hypothesis **H3***: learned predictions can be transferred to novel shapes.* Learners were trained on one or more objects, and tested on an object of different shape. Transfer was tested both in simulation and with real objects.

9.2 Experimental setup

In each trial the object was placed in a fixed location. Random pushes were generated as follows. A target point on the object surface was selected from a uniform distribution over the interval of the vertical plane intersecting with the object. This target contact point was then perturbed by a random angle of up to ± 10 degrees (Figure 9). The robot finger then moved along this straight line, for a distance l at constant speed. During the push, video and finger position were captured at 30Hz, including a 1 second buffer at either end of the finger trajectory. The object pose was tracked at 30Hz using a structural and texture edge based particle filter that is able to track in clutter and occlusion (Mörwald et al. 2009). Learning used the recovered pose of the object in every other frame (i.e. at 15Hz). For test trials the trajectory of the finger was known a priori and the object pose observed only at the initial frame. Using these a trajectory was predicted for the object over 150 steps at 15Hz (10 seconds). The predicted trajectory was created purely using the forward model and did not use any observations during the push to update its prediction. For real experiments, a 5-axis robot arm

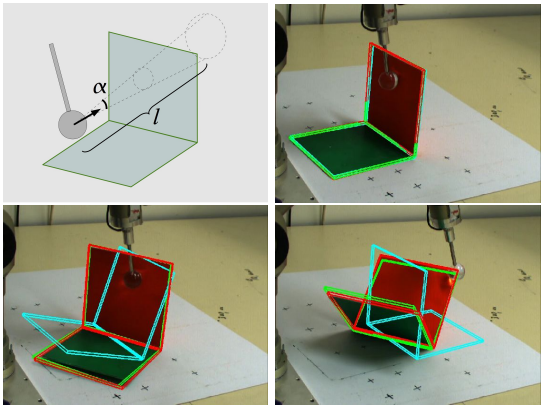

Fig. 9 In all experiments the robot finger pushes in a straight-line of length l=25±5 cm within a cone of angle α=20 deg toward an object (top left). The start point is randomised so that each region on the vertical face is equally likely to be pushed. The red wire-frame shows the output of the visual tracker, the green wire-frame the object pose predicted by the KDEF learner, and the blue wire-frame the prediction of the PhysX simulator.

with a single finger was used. Simulation experiments used the NVIDIA PhysX engine (NVIDIA PhysX 2009) to provide ground-truth. The PhysX engine was evaluated as a predictor itself in real object trials. All methods required the predictor to know the object shape model, represented as a mesh, and the starting pose. The correct model (context) was determined by fitting models from a library to the visual data. The visual context detector automatically picked the model and pose with the best visual fit according to our particle filter (Mörwald et al. 2009), converging to ±2mm error in the first few frames.

Local frames for environment contacts in the -GAE variants were fixed by hand to the edges of objects. In test cases with new objects the frames were again fixed by hand. An item for future work is to perform this process automatically. All methods required parameter tuning. Model selection was performed in experiment P1 to establish reasonable parameter values, which were then used in experiments P2 and P3. It was not possible to perform fully systematic optimisations for LWPR, KDE and KDEF due to the size of the parameter spaces. Rather, subsets of the parameter space were selected by inspection and then explored using grid search. Models were evaluated on a separate hold-out set, of the same size as the test set. Model selection by full grid search was performed for the following parameters of the PhysX simulator: static friction, dynamic friction and the coefficient of restitution. The full set of parameters is given in Table 2, leading to 125 different parameter combinations being tried for PhysX for each training object. PhysX has access to full mesh and contact information. Parameter search for the KDE methods was performed for the bandwidth of the kernels, with three values tried. For the KDE and LWPR methods, in addition to model selection the three different parameterisations (Gauss-Euler (e), Gauss-Quaternion (q), Von-Mises-Fisher-Quat (v)) of rotations for the density estimation method were studied in experiment P1, and subsequently the best solution was used in experiments P2 and P3. For LWPR we used the Euler parameterisation throughout experiments P1, P2 and P3. For experiment P1 we performed 10-fold cross-validation. The sizes of the training and test sets are stated in the method for each experiment. For transfer learning experiments P2 and P3, disjoint training and test sets were used. For clarity a complete set of acronyms for the algorithm-information combinations is given in Table 3.

9.3 Performance measure

In all experiments with real objects, predicted trajectories were evaluated against the visual tracked object pose. The tracker does not provide perfect ground-truth, yielding errors of ±2mm. Prediction performance is evaluated as follows.

At any particular time step, t, a large number, N, of randomly chosen points $p_n^{1,t}$, where $n = 1 \dots N$, are rigidly attached to an object at the ground-truth pose, and the corresponding points $p_n^{2,t}$ to an object at the predicted pose. At time step t, an average error E_t can now be defined as the mean of displacements between points on the object at the predicted pose and points on the object at the ground-truth pose:

$$E_t = \frac{1}{N} \sum_{n=1 \dots N} |p_n^{2,t} - p_n^{1,t}| \tag{21}$$

Note that for each push action, we predict approximately 150 consecutive steps into the future, with no recursive filtering or corrector steps, hence it is expected

Parameter	Values				
restitution	0.125	0.1875	0.25	0.375	0.5
static friction	0.25	0.3125	0.5	0.75	1.0
dynamic friction	0.25	0.3125	0.5	0.75	1.0

Table 2 Parameter settings for optimisation of PhysX.

	Information		
Predictor	G	G+A	G+A+E
LWPR	LWPR-G	LWPR-GA	LWPR-GAE
KDE	KDE-G	KDE-GA	KDE-GAE
KDEF	KDEF-G	KDEF-GA	KDEF-GAE
PhysX	n/a	n/a	n/a

Table 3 Algorithm-information variants.

that errors will grow with range from the initial object pose. We therefore find it more meaningful to normalise all errors with respect to an "average range", R_t, of the object from its starting position, defined as:

$$R_t = \frac{1}{N} \sum_{n=1\ldots N} |p_n^{1,t} - p_n^{1,0}| \tag{22}$$

For a test data set, consisting of K robotic pushes, each of which breaks down into many consecutive predictions over T time steps, we can now define average error and normalised average error. Note that the normalised error measure necessarily has no units.

$$E_{av} = \frac{1}{K} \sum_{k=1}^{K} \frac{1}{T} \sum_{t=1}^{T} E_t, \quad E_{av}^{norm} = \frac{1}{K} \sum_{k=1}^{K} \frac{1}{T} \sum_{t=1}^{T} \frac{E_t}{R_t} \tag{23}$$

10 Results

10.1 Experiment P1: Action Interpolation

In Experiment P1 the robot applied a set of random pushes to a polyflap, a box and a cylinder respectively. All the algorithm variants in Table 3 were trained and tested. Model selection was performed for all algorithm-information combinations including PhysX. Ten fold cross-validation was performed for all algorithms. The density estimation techniques were studied with all three parameterisations of rotation. Training (and testing) sets were 200 (25) pushes (cylinder), 400 (50) pushes (box) and 700 (90) pushes (polyflap). Figure 10 (left column) shows convergence of the best learning algorithms. Figure 10 (right column) shows how performance varies with input information for the best parameterisations of all the algorithms. Table 4 shows the results of model selection on the different parameterisations for KDE. Image sequences of predicted vs actual trajectories are shown in (Figure 13). For the simulation experiments on non-planar surfaces, 900 (100) pushes of a cylinder in two different starting positions (upright and on its side) were made. For this simulated experiment we only used factored KDE with the Gaussian-quaternion parameterisation, on the basis that this was the best performing setup for the real experiments.

10.1.1 Experiment P1 discussion

Table 4 and Figure 10 show that the learned models almost always outperformed physics simulation on the test set, with approximately one third the prediction error. Thus we find strong support for hypothesis H1. Regarding the parameterisation, Gaussian kernels with quaternions were best in 14 of 15 cases (Table 4 bold entries). Thus this parameterisation was used in experiments P2 and P3. In Figure 13 it can be seen that predictions were accurate and physically plausible for a variety of learning methods even over 150 steps. Note the physics simulator predicts incorrect turning of the cylinder when pushed (Figure 13 column 8). Additionally Figure 10 shows that additional information A or E gives no advantage for any algorithm in this experiment, indeed LWPR gets worse with more dimensions. This is in line with expectation, since no learning transfer is being attempted. Finally, Figure 11 and Figure 12 show that the approach is also able to learn predictive models for a cylinder in a variety of starting positions on an uneven surface. This includes predictions of flipping the object up, and the object rolling away once contact is lost.

10.2 Experiment P2: Action Transfer

Experiment P2 tests hypothesis H2: whether predictions can be transfered to novel actions. The training set was 900 pushes applied to an L shaped flap in one direction (Figure 6 top left). The test set was 100 pushes applied from the other side (Figure 6 top right). The same method was followed in simulation and with the real object. All the algorithm-information variants in Table 3 were tested. We measured the transfer prediction error, i.e. the prediction error for the novel test actions. Figure 14 shows the normalised average error E_{av}^{norm} for the simulation experiment (left panel) and with real objects (right panel). Figure 15 shows example predicted trajectories on synthetic and real test cases.

10.2.1 Experiment P2 discussion

Figure 14 (left panel) shows that in simulation that additional contact information (A or AE) didn't improve performance of KDE and LWPR. In contrast, factorisation could take advantage of the additional information: the performance of KDEF improved significantly. The predictions of KDEF (Figure 15) precisely match the hypothesized effects of adding contact information depicted in Figure 6 (bottom row). With only global information the finger was predicted by KDEF to pass through the object (Figure 15 column 1). By adding the agent-object information the prediction of KDEF was that the object would move with the finger, but that it penetrated the table (Figure 15 column 2). By also adding object-environment information KDEF predicts that the object will slide along the table in contact with the finger (Figure 15 column 3). On real objects (Figure 14 right panel) the learned predictors slightly

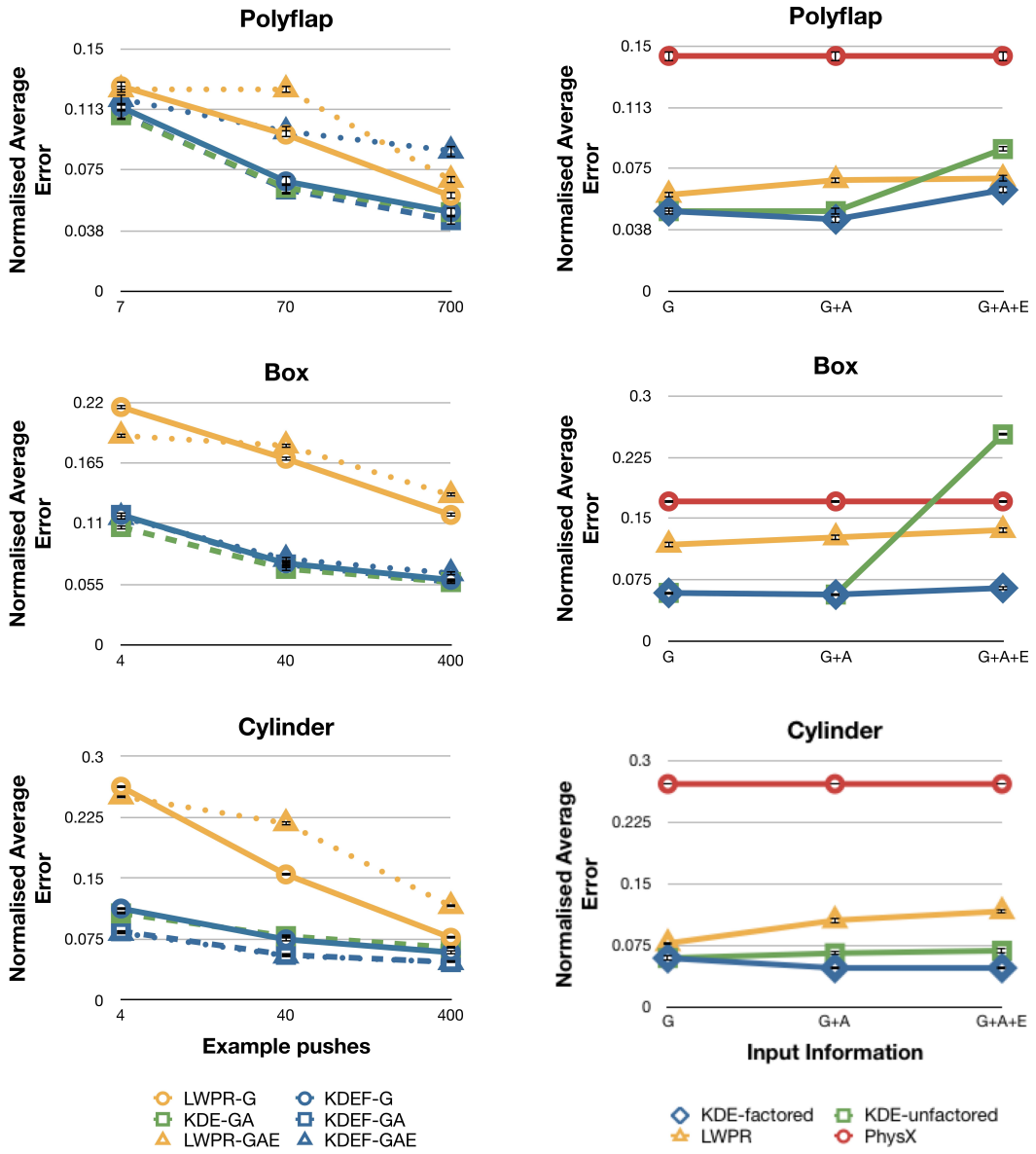

Fig. 10 Experiment P1: Convergence of a selection of learning algorithm-information combinations (left column). Change in normalised average prediction errors with varying input information (right column). G - global information; A - agent-object information; E - object-environment information. Standard error bars are shown in black, in most cases these are very small and fall within the symbol for each data point. We show error bars for all data points except for the learning convergence graph shown here.

outperform the physics engine, and prediction accuracy declines. Additional contact information with factoring still enables KDEF to make physically plausible predictions. Figure 15 (columns 5 and 6) shows that KDEF-G and LWPR-G predict that the finger passes through the object, and that the object doesn't move. In Figure 15 (columns 4 and 7) KDEF-GA correctly predicts the sliding motion of the object. Only factoring enables this, the unfactored methods don't produce plausible predictions. This supports hypothesis H2: factoring enables action transfer. Transfer is best if the training observations are accurate, diminishing with training noise.

10.3 Experiment P3: Shape Transfer

Experiment P3 tests hypothesis H3: can predictors that have been learned from one set of objects transfer their predictions to an object of novel shape? The experiment was run in simulation and with real objects. Shape transfer was tested from i) a polyflap to a box (P3.A) and ii) a box and a cylinder to a double cylinder (P3.B). There were 900 training pushes on the polyflap and 200 test pushes on the box for i), and 200 training pushes (100 box, 100 cylinder) and 100 test pushes (double cylinder) for ii). This experiment ran on real objects for

Predictor	Polyflap	Box	Cylinder
KDEF-Ge	0.055±0.002	0.061±0.003	0.063±0.003
KDEF-Gq	**0.049**±0.002	**0.059**±0.002	**0.059**±0.003
KDEF-Gv	0.057±0.002	0.066±0.003	0.071±0.003
LWPR-Ge	0.059±0.002	0.118±0.003	0.077±0.003
KDEF-GAe	0.054±0.002	0.060±0.003	0.052±0.002
KDEF-GAq	**0.044**±0.002	**0.057**±0.002	**0.047**±0.002
KDEF-GAv	0.064±0.002	0.097±0.002	0.109±0.003
LWPR-GAe	0.068±0.002	0.127±0.003	0.105±0.002
KDEF-GAEe	0.083±0.003	0.065±0.003	0.050±0.002
KDEF-GAEq	**0.062**±0.002	**0.065**±0.003	**0.047**±0.002
KDEF-GAEv	0.081±0.002	0.086±0.002	0.065±0.002
LWPR-GAEe	0.069±0.002	0.136±0.003	0.116±0.003
KDE-GAe	0.053±0.002	0.057±0.002	0.068±0.003
KDE-GAq	**0.049**±0.002	**0.057**±0.002	**0.065**±0.003
KDE-GAv	0.062±0.002	0.058±0.002	0.092±0.004
KDE-GAEe	0.090±0.002	0.161±0.003	0.071±0.003
KDE-GAEq	**0.087**±0.002	0.253±0.002	**0.068**±0.003
KDE-GAEv	**0.087**±0.002	**0.127**±0.003	0.091±0.004
PhysX	0.144±0.003	0.171±0.003	0.271±0.001

Table 4 Experiment P1: Forward push on a polyflap/box/cylinder, trained on real data. Shown is the dimensionless measure normalised average error E_{av}^{norm}± standard error. The parameterisations are denoted by e (Euler), q (Gauss Quaternion) and v (Gauss+Von-Mises Fisher) respectively.

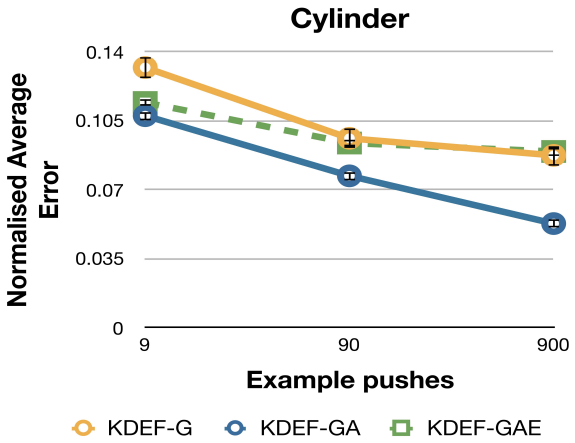

Fig. 11 Experiment P1: Convergence of learning for a cylinder on an uneven surface.

i) and ii) and in simulation for i), giving three train-test conditions in total. All algorithm-information combinations in Table 3 were tried. When learning from two objects the same number of factors (experts) were used for each object, and they were matched across the two objects by hand. Thus each expert received a mix of data from each object, learning to encode rolling, sliding or tipping motions. The normalised average error for all three conditions E_{av}^{norm} is shown in Figure 16. Example frames are shown in Figure 17.

10.3.1 Experiment P3 discussion

Shape transfer only occurs with contact information and factoring, such as for the KDEF-GA method in experiment P3.A (Figure 17 column 1). Learners with global information predict that the finger passes through the box (Figure 17 columns 2 and 3). In experiment P3.A only factoring plus all the contact information (KDEF-GAE) produced physically plausible predictions. In Figure 17 (column 6) KDEF-GAE predicts that the double cylinder will slide along the table, whereas KDEF-G and KDEF-GA predict it will penetrate the table (Figure 17 columns 4 and 5). KDEF-GAE also makes physically plausible predictions for a novel real object (Figure 17 column 7). None of the other learners could achieve this shape transfer learning. Only by using factoring plus all contact information was shape transfer learning achieved. In fact KDEF-GAE also matched the accuracy of the physics simulator. Thus this experiment supports hypothesis H3: factoring + contact information enables shape transfer learning.

10.4 General Discussion

There are two questions that arise from the experiments collectively. First why does PhysX fail to do better in P1 even though separately tuned to each object? The answer is that real objects don't adhere to idealised friction models with one coefficient for each surface: flaws in object surfaces cause deviations from the tuned model. Thus the problem holds for all such simulators and so a modular learning model will always be better. Second, why does transfer learning decline on real data in P2 and P3? The answer is tracking noise in the training data, leading to perceived penetrations of the object by the finger, giving some probability in the model that the finger can pass through the object.

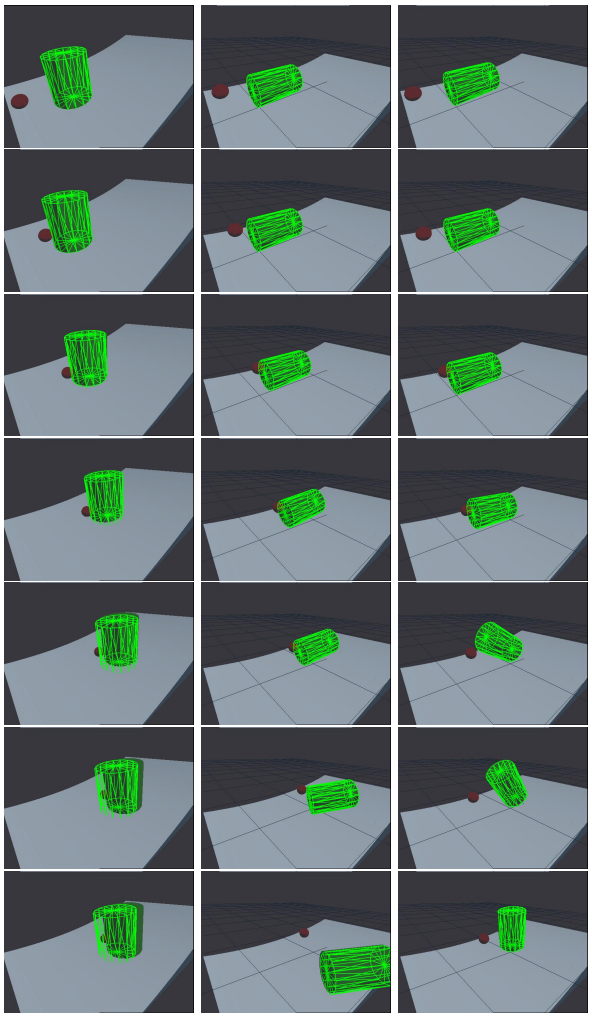

Fig. 12 Experiment P1: predictions for a simulated cylinder on a non-planar surface. Predictions were made over 150 steps by the KDEF-GA/quat method. Note that the learned model can correctly predict for two starting orientations, and for dynamic flipping and rolling motions once the finger loses contact.

11 Related Work

Related work is split into four broad areas: neuroscience, analytic approaches, qualitative physics and machine learning. Prediction of motor effects on the body has long been studied in neuroscience (Miall and Wolpert 1996; Flanagan et al. 2003). MOSAIC was an early computational model of prediction and control in the cerebellum using a modular scheme (Haruno et al. 2001), where predictions can be made by convex combinations of learned predictors. Other bio-inspired modular prediction schemes were independently derived by roboticists (Demiris and Khadhouri 2006). These models all differ from ours in that our work is the first attempt at learning to model the motions of objects with kinematic constraints. There is also evidence that infants can learn object specific motions (Bahrick and Pickens 1995). It is also clear that while some object knowledge may be innate (Spelke et al. 1994), object specific predictions must be learned, and are critical to our manipulation skills (Flanagan et al. 2006). So in general terms modular learning of predictions of object behaviour is cognitively plausible.

There is substantial work in robotics on classical analytic mechanics models of pushing (Mason 1982; Lynch 1992; Peshkin and Sanderson 1988; Cappelleri et al. 2006), on both kinematic and dynamic models of manipulation effects (Mason 2001). Such analytic models are good metric predictors if their key parameters (e.g. friction) are precisely known, although qualitative predictions are robust to parameter uncertainty. They can also inform push planning under pose uncertainty (Brost 1985). These approaches are appealing in that proofs concerning the qualitative object motion can be obtained, particularly under quasi-static conditions (Mason and Salisbury 1985; Peshkin and Sanderson 1988). This led to methods for push planning that have some guarantees, such as completeness and optimality (Lynch and Mason 1996). There is a separate body of work on qualitative models of action effects on objects, rooted in naive physics (Hayes 1995), and qualitative physics (Kuipers 1986). In a similar spirit there is work on using physics engines to learn qualitative action effects (Mugan and Kuipers 2012), and high level planning of manipulation (Stilman and Kuffner 2008; Roy et al. 2004) using qualitative action models. Some early ideas on push planning have reappeared in recent robots that plan pushes to enable grasps in clutter (Dogar and Srinivasa 2010).

Learning for forward modelling has been long understood (Jordan and Jacobs 1990; Jordan and Rumelhart 1992). In robotics it has been used model contactless motion, e.g. predicting the motion of an object, robot arm, or gripper in free space (Ting et al. 2006; Boots et al. 2014; Dearden and Demiris 2005). The next step was to learn the dynamics of an object with a single, constant contact (such as pole balancing) (Schaal 1997; Atkeson and Schaal 1997). Finally there has been work on affordance learning, and on which variables are relevant to predicting object motion (Montesano et al. 2008; Moldovan et al. 2012; Hermans et al. 2011; Fitzpatrick et al. 2003; Ridge et al. 2010; Kroemer and Peters 2014). The restriction of each of these papers is that they make qualitative predictions of object motion, such as a classification of the type of motion outcome. There has also been work on predicting stable push locations (Hermans et al. 2013). Finally there has been recent work in which metric motion models are learned from experience. Stoytchev (Stoytchev 2008) enabled

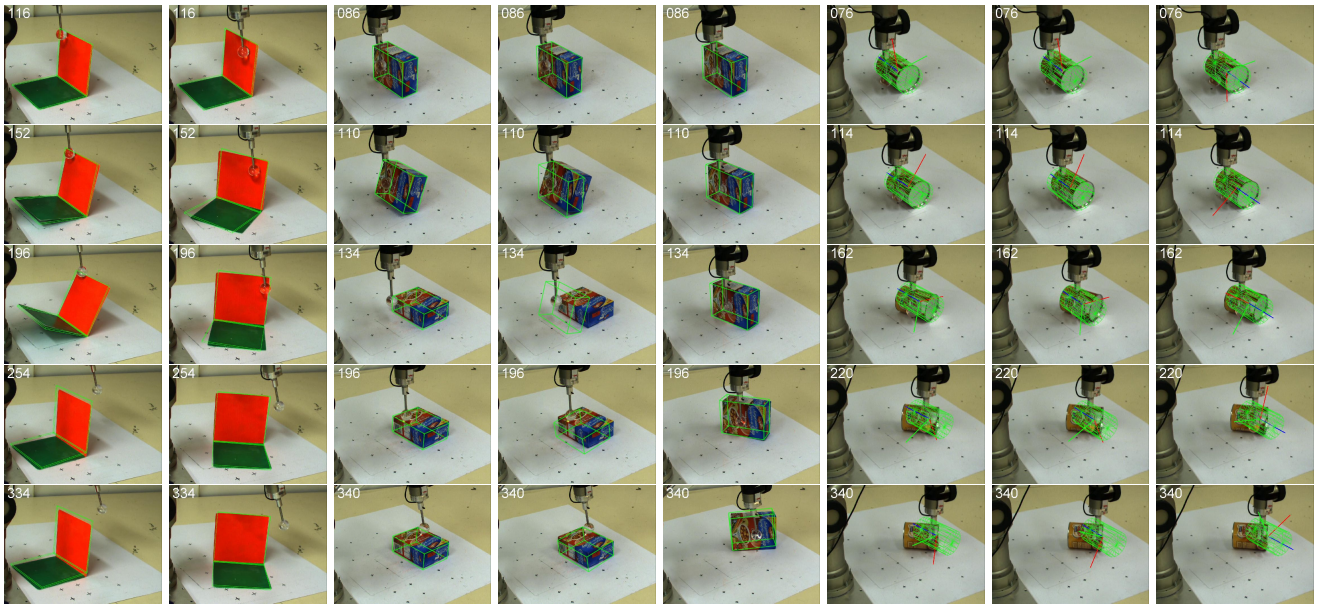

Fig. 13 Experiment P1: polyflap, box and cylinder. Green outline shows predictions. Columns 1-2: KDEF-GA/quat on two trials exhibiting different motions of the polyflap. Col 3: KDEF-GA/quat. Col 4: LWPR-G for one trial in which the box topples over. Col 5: KDEF-GA/quat on another trial in which the box slides. Columns 6-8 show the same push of the cylinder. Col 6: KDEF-GA/quat. Col 7: LWPR-G. Col 8: PhysX. Note tha for columns 6-7 the orientation of the cylinder is show by the rotating frame. Only the learned models predict the rotation correctly. Frame numbers are in the top left of each image.

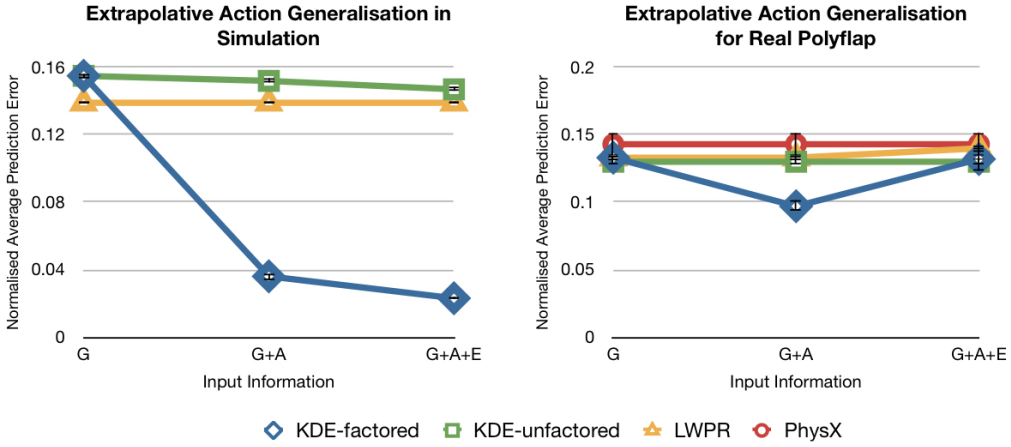

Fig. 14 Experiment P2: Action transfer. Trained on forward push on polyflap, tested on backward push, for simulated (top) and real data (bottom). Comparative performance of predictors vs. information utilised (global/agent/environment), as measured by normalised average error E_{av}^{norm}.

a robot to learn action effects of sticks and hook-like tools by pushing objects. This work simplifies the domain by using circular pucks as objects, and four planar motions as actions. Action outcomes were learned for various tools in a modular fashion, but without transfer learning. In both (Meriçli et al. 2014) and Scholz and Stilman (2010) the metric planar motion of pushed objects on the plane is learned, and the learning is modular (per object) as here. In each case a small number of discrete pushing actions is tried, motion models are planar, rather than full rigid body transformations.

Our work sits at the intersection of some these approaches. We embrace machine learning and modularity to achieve scalability, but we also explicitly model each contact. Our machine learning approach is used to make metrically precise predictions, under contact, including changing contact with the environment. In this way we try to re-achieve in a machine learning framework what only the analytic approach has attempted to date: metric prediction of motion transferable to novel actions and objects.

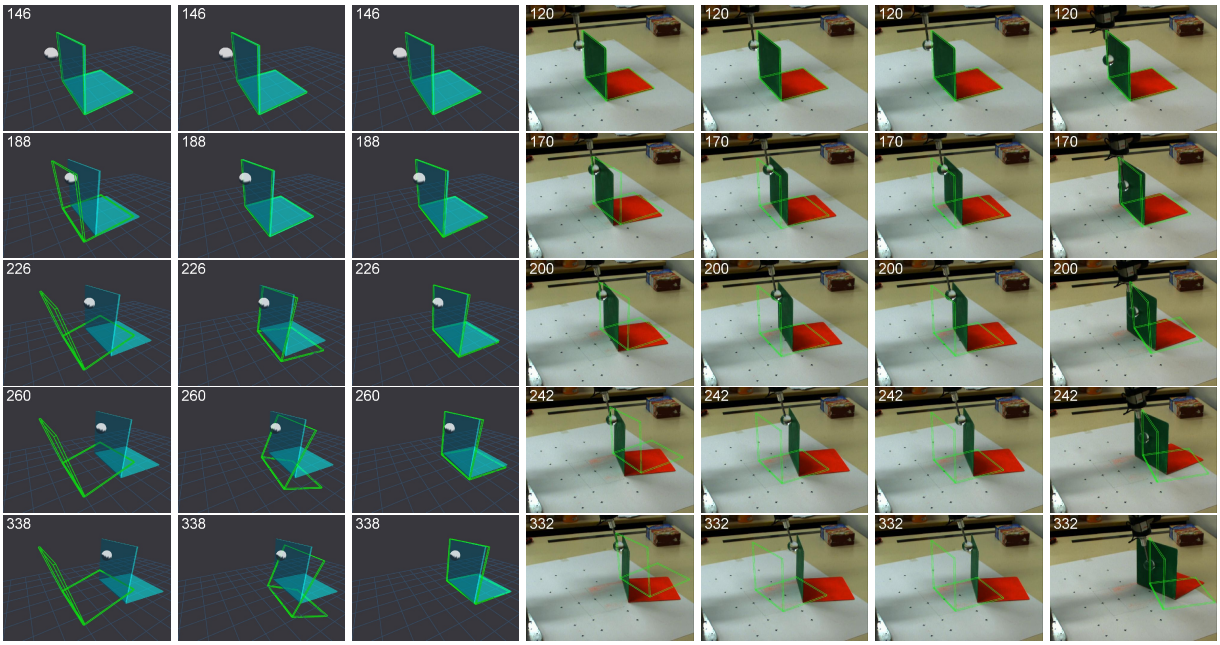

Fig. 15 Experiment P2: Green outline shows predictions. Column 1: KDEF-G/quat. Col 2: KDEF-GA/quat. Col 3: KDEF-GAE/quat. Col 4: KDEF-GA/quat. Col 5: KDEF-G/quat. Col 6: LWPR-G. Col 7: KDEF-GA/quat. Note that the KDEF-G/quat and LWPR-G methods predict that the robot finger passes through the polyflap. Frame numbers are in the top left of each image.

12 Conclusions

This paper has found that: modular predictors of object motion can be learned; learning transfer is possible; contact information assists transfer; factorisation helps to exploit this information; and learning can exceed or match physics engine performance. The paper presented the first results on real objects for object transfer. What do these results tell us about the way to proceed? What is the space of methods for prediction? We note the following issues.

12.0.1 Prior knowledge

While the prior knowledge embodied by classical mechanics provides generality, the necessary approximations made in implementations can hinder accurate prediction. Rigid body simulators also require learning of the intrinsic parameters of the object, but sometimes have too many constraints to wrap themselves finely around real data. On the other hand it is clear that some structural knowledge is required: contact information is structural knowledge benefiting transfer. Pure tabula rasa learning is unlikely to be the answer.

12.0.2 Local shape

The learners employed here used much less information than the full object shape. Further shape information might improve prediction further. Specifically, the local surface shapes of both surfaces at a contact influence object motion. Experts specialised to local shape contexts may improve prediction performance. In the scheme presented here, this would result in nesting another modular structure inside the product of experts. It would also provide a means to solve the problem of how to automatically attach experts to objects.

12.0.3 Modularity

There is evidence that the brain employs modularity in prediction, and in developing expert motor skills. We have argued that this is a promising way to proceed for robotics. Rather than learning a general purpose predictor, why not learn very many, very specific predictors? Memory in current computing technology is cheap, and so learning many hundreds or even thousands of object specific prediction modules is feasible. Modularity is part of the way to proceed.

12.0.4 Multiple changing contacts

In manipulation, the hand makes multiple, changing contacts with the object. Prediction for manipulation must account for these non-smooth changes. Hybrid models may be a way to proceed. These have been explored in modelling changing contact dynamics in walking, but have yet to be applied to manipulation.

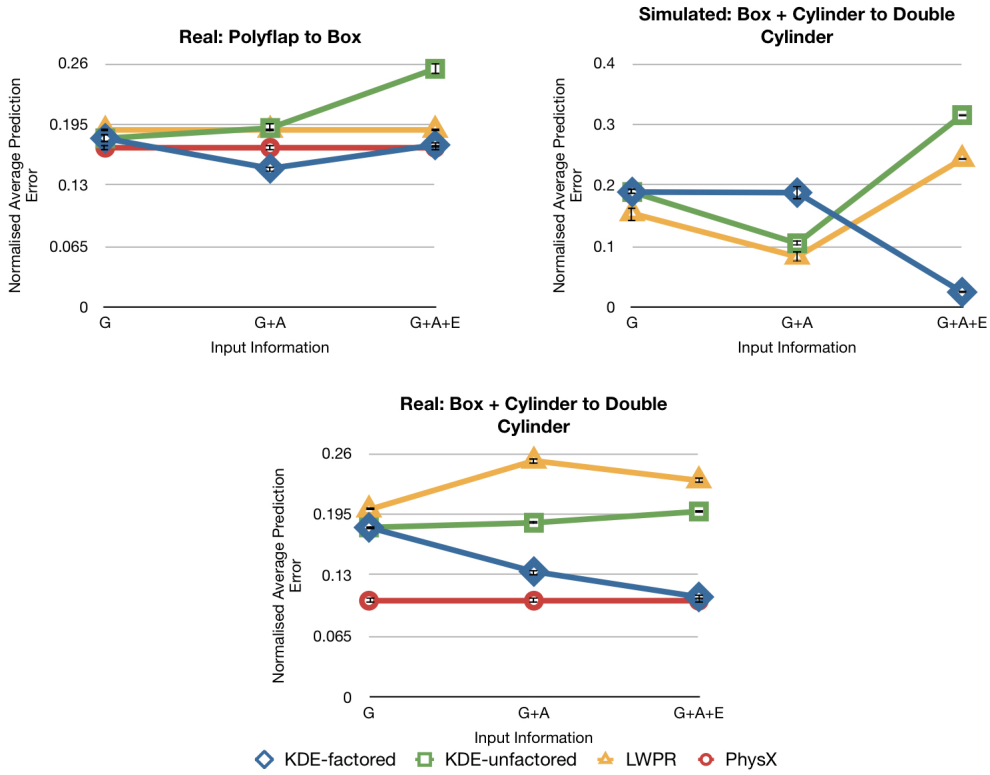

Fig. 16 Experiment P3: Comparative performance of predictors vs. information utilised, as measured by the normalised average error E_{av}^{norm}.

12.0.5 Training noise

Transfer performance in the approach presented here degrades under training noise. Recently, we have partially addressed this by removing noise at prediction time using kinematic optimisation Belter et al. (2014). This combines the benefits of collision detection with the benefits of machine learning, and improves prediction performance significantly. It is, however, unclear as to whether the learned models are then transferrable to novel objects or actions. Thus, whether this approach is extensible is an open question.

12.0.6 Dynamics

We have restricted this study to quasi-static cases, but the formulation of the basic regression problem with dynamics was given. Learning with dynamics is the next obvious step.

References

Abramowitz, M., Stegun, I.A.: (1965). *Handbook of Mathematical Functions: With Formulas, Graphs, and Mathematical Tables*. Dover, NY

Atkeson, C.G., Schaal, S.: (1997). Learning tasks from a single demonstration. In: *Robotics and Automation, 1997. Proceedings., 1997 IEEE International Conference on*, vol. 2, pp. 1706–1712. IEEE

Bahrick, L.E., Pickens, J.N.: (1995). Infant memory for object motion across a period of three months: Implications for a four-phase attention function. *Journal of Experimental Child Psychology* **59**(3), 343 – 371

Belter, D., Kopicki, M., Zurek, S., Wyatt, J.: (2014). Kinematically optimised predictions of object motion. In: *Proceedings of the IEEE/RSJ International Conference on Intelligent Robotics and Systems (IROS 2014)*, pp. 4422–4427

Boots, B., Byravan, A., Fox, D.: (2014). Learning predictive models of a depth camera and manipulator from raw execution traces. In: *Proceedings of the IEEE International Conference on Robotics and Automation (ICRA 14)*, pp. 4021–4028. IEEE

Brost, R.C.: (1985). Planning robot grasping motions in the presence of uncertainty. Tech. Rep. CMU-RI-1R-85-12

Cappelleri, D.J., Fink, J., Mukundakrishnan, B., Kumar, V., Trinkle, J.C.: (2006). Designing open-loop plans for planar micro-manipulation. In: *Proceedings of the IEEE International Conference on Robotics and Automation (ICRA 2006)*, pp. 637–642

Cheng, Y.: (1995). Mean shift, mode seeking, and clustering. *IEEE Transactions on Pattern Analysis and Machine Intelligence* **17**(8), 790–799

Cosgun, A., Hermans, T., Emeli, V., Stilman, M.: (2011). Push planning for object placement on cluttered table surfaces. In: *Proceedings of the IEEE/RSJ International*

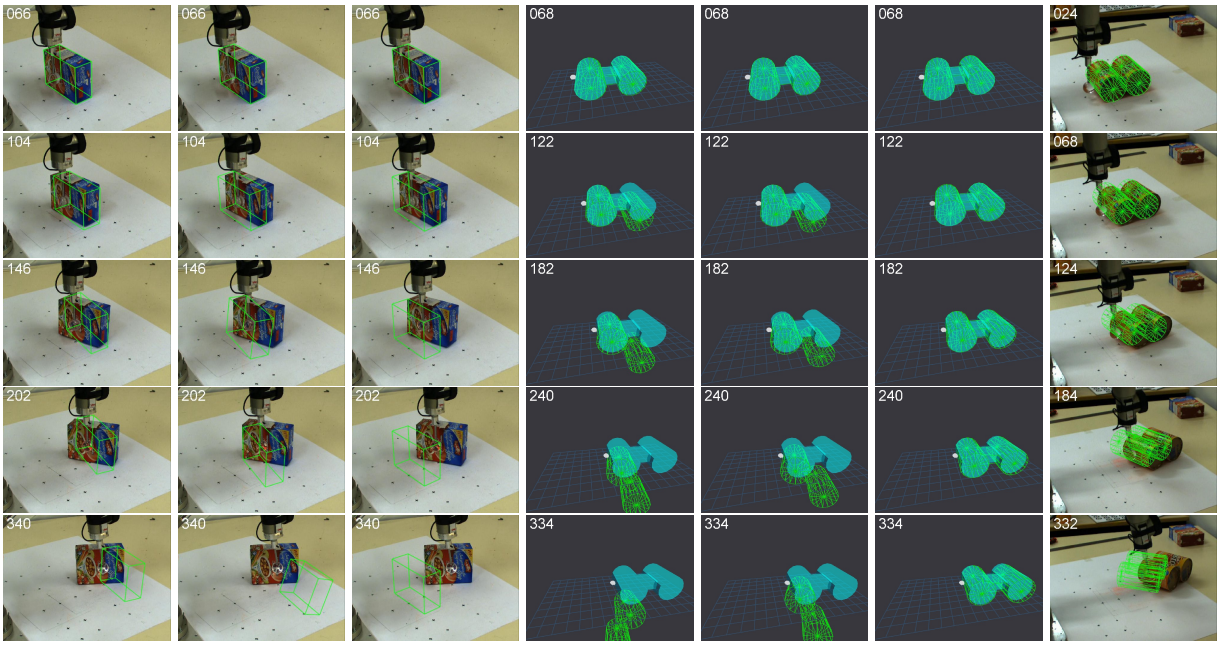

Fig. 17 Experiment P3: Shape Transfer. Green outline shows predictions. Column 1: KDEF-GA/quat. Col 2: KDEF-G/quat. Col 3: LWPR-G for one trial. Note that the KDEF-G/quat and LWPR-G methods predict that the robot finger moves into the box. Col 4: KDEF-G/quat. Col 5: KDEF-GA/quat. Col 6: KDEF-GAE/quat. Col 7: KDEF-GAE/quat. Frame numbers are in the top left of each image.

Conference on Intelligent Robotics and Systems (IROS 2011), pp. 4627–4632. IEEE

Craik, K.J.W.: (1943). *The nature of explanation.* CUP Archive

Dearden, A., Demiris, Y.: (2005). Learning forward models for robots. In: *Proceedings of the International Joint Conference on Artificial Intelligence (IJCAI 2005)*, vol. 5, p. 1440

Demiris, Y., Johnson, M.: (2003). Distributed, predictive perception of actions: a biologically inspired robotics architecture for imitation and learning. *Connection Science* **15**(4), 231–243

Demiris, Y., Khadhouri, B.: (2006). Hierarchical attentive multiple models for execution and recognition of actions. *Robotics and Autonomous Systems* **54**(5), 361–369

Detry, R.: (2010). *Learning of multi-dimensional, multi-modal features for robotic grasping.* Ph.D. thesis, University of Liege

Dogar, M., Srinivasa, S.: (2010). Push-grasping with dexterous hands: Mechanics and a method. In: *Proceedings of the IEEE/RSJ International Conference on Intelligent Robotics and Systems (IROS 2010)*, pp. 2123–2130

Fitzpatrick, P., Metta, G., Natale, L., Rao, S., Sandini, G.: (2003). Learning about objects through action-initial steps towards artificial cognition. In: *Proceedings of the IEEE International Conference on Robotics and Automation (ICRA 2003)*, vol. 3, pp. 3140–3145

Flanagan, J.R., Bowman, M.C., Johansson, R.S.: (2006). Control strategies in object manipulation tasks. *2006* **16**, 650–659

Flanagan, J.R., Vetter, P., Johansson, R.S., Wolpert, D.M.: (2003). Prediction precedes control in motor learning. *Current Biology* **13**, 146–150

Flickinger, D.M., Williams, J., Trinkle, J.C.: (2015). Performance of a method for formulating geometrically exact complementarity constraints in multibody dynamic simulation. *Journal of Computational and Nonlinear Dynamics* **10**(1), 011,010–011,010–12

Haruno, M., Wolpert, D.M., Kawato, M.: (2001). Mosaic model for sensorimotor learning and control. *Neural Computation* **13**, 2201–2220

Hayes, P.J.: (1995). The second naive physics manifesto. In: *Computation & intelligence*, pp. 567–585. AAAI

Hermans, T., Li, F., Rehg, J.M., Bobick, A.F.: (2013). Learning contact locations for pushing and orienting unknown objects. In: *Proceedings of the IEEE-RAS International Conference on Humanoid Robotics*, pp. 435–442

Hermans, T., Rehg, J., Bobick, A.: (2011). Affordance prediction via learned object attributes. In: *ICRA 2011: Workshop on Semantic Perception, Mapping, and Exploration*

Johansson, R.J., Cole, K.J.: (1992). Sensory-motor coordination during grasping and manipulative actions. *Current Opinion in Neurobiology* **2**, 815–823

Jordan, M.I., Jacobs, R.A.: (1990). Learning to control an unstable system with forward modeling. In: *Advances in Neural Information Processing Systems*, pp. 324–331

Jordan, M.I., Rumelhart, D.E.: (1992). Forward models: Supervised learning with a distal teacher. *Cognitive Science* **16**, 307–354

Klanke, S., Vijayakumar, S., Schaal, S.: (2008). A library for locally weighted projection regression. *The Journal of Machine Learning Research* **9**, 623–626

Kopicki, M.: (2010). *Prediction learning in robotic manipulation.* Ph.D. thesis, University of Birmingham

Kopicki, M., Wyatt, J., Stolkin, R.: (2009). Prediction learning in robotic pushing manipulation. In: *Proceedings of the IEEE International Conference n Advanced Robotics (ICAR 2009)*, pp. 1–6

Kopicki, M., Zurek, S., Mörwald, T., Wyatt, J.: (2011). Learning to predict how rigid objects behave under simple manipulation. In: *Proceedings of the IEEE International Conference on Robotics and Automation (ICRA 2011)*

Kroemer, O., Peters, J.: (2014). Predicting object interactions from contact distributions. In: *Proceedings of the IEEE/RSJ International Conference on Intelligent Robotics and Systems (IROS 2014)*

Kuipers, B.: (1986). Qualitative simulation. *Artificial Intelligence Journal* **29**(3), 289–338

Lynch, K.: (1992). The mechanics of fine manipulation by pushing. In: *Proceedings of the IEEE International Conference on Robotics and Automation (ICRA 1992)*, pp. 2269–2276

Lynch, K.M., Mason, M.T.: (1996). Stable pushing: Mechanics, controllability, and planning. *International Journal of Robotics Research* **15**, 533–556

Mason, M.T.: (1982). *Manipulator grasping and pushing operations*. PhD thesis, MIT

Mason, M.T.: (2001). *Mechanics of robotic manipulation*. MIT press

Mason, M.T., Salisbury, J.K.: (1985). *Robot hands and the mechanics of manipulation*. The MIT Press, Cambridge, MA

Mehta, B., Schaal, S.: (2002). Forward models in visuomotor control. *Journal of Neurophysiology* **88**, 942–953

Meriçli, T., Veloso, M., Akın, H.L.: (2014). Push-manipulation of complex passive mobile objects using experimentally acquired motion models. *Autonomous Robots* **38**(3), 317–329

Miall, R., Wolpert, D.: (1996). Forward models for physiological motor control. *Neural Networks* **9**(8), 1265 – 1279

Moldovan, B., Moreno, P., van Otterlo, M., Santos-Victor, J., Raedt, L.D.: (2012). Learning relational affordance models for robots in multi-object manipulation tasks. In: *Proceedings of the IEEE International Conference on Robotics and Automation (ICRA 2012)*, pp. 4373–4378

Montesano, L., Lopes, M., Bernardino, A., Santos-Victor, J.: (2008). Learning object affordances: From sensory-motor coordination to imitation. *IEEE Transations on Robotics* **24**(1), 15–26

Mörwald, T., Zillich, M., Vincze, M.: (2009). Edge tracking of textured objects with a recursive particle filter. In: *Proc. of Graphicon*

Mugan, J., Kuipers, B.: (2012). Autonomous learning of high-level states and actions in continuous environments. *IEEE Transactions on Autonomous Mental Development* **4**(1), 70–86

Murray, R., Li, Z., Sastry, S.: (1994). *A mathematical introduction to robotic manipulation*. CRC press

NVIDIA PhysX: Physics simulation for developers (2009). URL http://http://developer.nvidia.com/physx

Peshkin, M., Sanderson, A.: (1988). The motion of a pushed, sliding workpiece. *IEEE Journal on Robotics and Automation* **4**, 569–598

Ridge, B., Skocaj, D., Leonardis, A.: (2010). Self-supervised cross-modal online learning of basic object affordances for developmental robotic systems. In: *Proceedings of the IEEE International Conference on Robotics and Automation (ICRA 2010)*, pp. 5047–5054

Roy, D., Hsiao, K.Y., Mavridis, N.: (2004). Mental imagery for a conversational robot. *Systems, Man, and Cybernetics, Part B: Cybernetics, IEEE Transactions on* **34**(3), 1374–1383

Schaal, S.: (1997). Learning from demonstration. In: *Advances in Neural Information Processing Systems 9*, pp. 1040–1046.

Scholz, J., Stilman, M.: (2010). Combining motion planning and optimization for flexible robot manipulation. In: *Humanoid Robots (Humanoids), 2010 10th IEEE-RAS International Conference on*, pp. 80–85. IEEE

Scott, D.W., Sain, S.R.: (2004). *Multi-Dimensional Density Estimation*, pp. 229–263. Elsevier

Spelke, E.S., Katz, G., Purcell, S.E., Ehrlich, S.M., Breinlinger, K.: (1994). Early knowledge of object motion: Continuity and inertia. *Cognition* **51**(2), 131–176

Stilman, M., Kuffner, J.J.: (2008). Planning among movable obstacles with artificial constraints. *International Journal of Robotics Research* **27**(12), 1296–1307

Storn, R., Price, K.: (1997). Differential evolution - a simple and efficient heuristic for global optimization over continuous spaces. *Journal of Global Optimization* **11**(4), 341–359

Stoytchev, A.: (2008). Learning the affordances of tools using a behavior-grounded approach. *LNAI* **4760**, 140–158

Ting, J.A., Mistry, M., Peters, J., Schaal, S., Nakanishi, J.: (2006). A Bayesian approach to nonlinear parameter identification for rigid body dynamics. In: *Robotics: Science and Systems*

Vijayakumar, S., D'souza, A., Schaal, S.: (2005). Incremental online learning in high dimensions. *Neural Computation* **17**(12), 2602–2634

Witney, A.G., Goodbody, S.J., Wolpert, D.M.: (2000). Learning and decay of prediction in object manipulation. *Journal of Neurophysiology* **84**(1), 334–343

Zito, C., Stolkin, R., Kopicki, M., Wyatt, J.L.: (2012). Two-level RRT planning for robotic push manipulation. In: *Proceedings of the IEEE/RSJ International Conference on Intelligent Robotics and Systems (IROS 2012)*, pp. 678–685. IEEE